Mon. Not. R. Astron. Soc. **000**, 000–000 (0000) Printed 1 June 2009 (MN LATEX style file v2.2)

# Gas phase mean opacities for varying [M/H], N/O, and C/O

Ch. Helling⋆ and W. Lucas
*SUPA, School of Physics and Astronomy, University of St Andrews, North Haugh, St Andrews, KY16 9SS, UK*



1 June 2009

**ABSTRACT**

We present a set of gas-phase Planck mean and Rosseland mean opacity tables applicable for simulations of star and planet formation, stellar evolution, disk modelling at various metallicities in hydrogen-rich environments. The tables are calculated for gas temperatures between 1000K and 10000K and total hydrogen number densities between $10^2$ cm$^{-3}$ and $10^{17}$ cm$^{-3}$. The carbon-to-oxygen ratio is varied from 0.43 to well above 2.0, the nitrogen-to-oxygen ration between 0.14 and 100.0. The tables are calculated for a range of metallicities down to [M/H]$'$ = $\log N_{\rm M}/N_{\rm H}$ = −7.0. We demonstrate how the mean opacities and the abundances of the opacity species vary with C/O, N/O, and [M/H]$'$. We use the element abundances from Grevesse, Asplund & Sauval (2007), and we provide additional tables for the oxygen-abundance value from Caffau et al.(2008). All tables will be available online under http://star-www.st-and.ac.uk/~ch80/datasources.html.

**Key words:** molecular data, radiative transfer, (stars:) planetary systems: protoplanetary discs, stars: formation , methods: numerical

## 1 INTRODUCTION

Star and planet formation modelling (e.g. Wuchterl 2005), stellar evolution modelling (e.g. Marques, Monteiro & Fernandes 2008, VandenBerg et al. 2008), galactic evolution modelling (e.g. Mollá et al. 2007) remain dependent on the availability of opacity data. Often, the mean opacities were only available on very sparse temperature-density grids (Wuchterl 2003; priv. com.). Intermediate mass asymptotic Giant Branch (AGB) stars develop from oxygen-rich (C/O<1) into carbon-rich (C/O>1) and are a major source of element enrichment of the insterstellar medium (ISM) (e.g. Gail & Sedlmayr 1986, Dominik et al. 1990, Dorfi & Höfner 1998, Wachter et al. 2008). However, mass-loss formulae describing the matter return from the AGB stars into the ISM do still model the gas opacity by a constant values (Wachter et al. 2008).The modelling of single stars does allow the treatment of a frequency dependent radiative transfer also in dynamic models for carbon-rich (Höfner et al. 2003, Gautschy-Loidl et al. 2004, Nowotny et al. 2005) and oxygen-rich (Woitke 2006) pulsating AGB stars . Extremely metal-poor giant stars with a metallicity of [M/H]$\lesssim -3.5$ (Cohen et al. 2008, Cayrel et al. 2004) seem to provide strong constrains on the element yields of first super-novae (SN) into the ISM (e.g. Cayrel et al. 2004). Therefore, the need for gas-phase opacity tables for a wider range of metallicities ([M/H]), carbon-to-oxygen ratios (C/O), but also nitrogen-to-oxygen ratios (N/O) has grown with the new challenge to model the evolution of star formation at high z, i.e. in a comparably young universe with stars containing much less elements than our Sun. The actual determination of the element abundances profs difficult (see Tsuji 2008) and is particular severe for the solar values (Grevesse, Asplund & Sauval 2007, Caffau et al. 2008) which are used as reference throughout astronomy. Furthermore, we need to be aware that stars in other galaxies can have an abundance patters different to the Sun e.g. due to a different star formation history (e.g. Koch et al. 2008). Helling, Winters & Sedlmayr (2000) presented the differences in the gas-phase mean opacities for the small and the large Magellanic cloud which element abundances clearly differ from that of the Sun. Based on this early work on mean opacities for AGB star wind models, we provide an extensive grid of mean opacity tables with an increased number of line opacity species (Sect. 2.2) for varying [M/H]$'$, C/O, and N/O (Sect. 2.3 and 3). We investigate the influence of these parameters on the Planck and the Rosseland mean gas-phase opacities, and the influence of the oxygen abundance values on our mean opacities stimulated by the ongoing discussion (Sect. 3).

## 2 METHOD

### 2.1 Mean opacity formulae

We compute mean opacity tables in the Rosseland mean approximation,

$$(\kappa_{\rm Ross})^{-1} = \sum_{\rm i}^{\rm N} \left\{ \frac{\int_0^\infty \frac{1}{n_{\rm i}(\rho,T)\,\kappa_\nu^{\rm i}(T)} \frac{\partial B_\nu(T)}{\partial T}\, d\nu}{\int_0^\infty \frac{\partial B_\nu(T)}{\partial T}\, d\nu} \right\}, \quad (1)$$

and the Planck mean approximation,

$$\kappa_{\rm Planck} = \sum_{\rm i}^{\rm N} n_{\rm i}(\rho,T) \left\{ \frac{\int_0^\infty \kappa_\nu^{\rm i}(T)\, B_\nu(T)\, d\nu}{\int_0^\infty B_\nu(T)\, d\nu} \right\}, \quad (2)$$

⋆ E-mail: Christiane.Helling@st-and.ac.uk

with $B_\nu(T)$ the Planck function at frequency $\nu$ and local temperature $T$ in [K]. $n_\mathrm{i}$ is the number density in [cm$^{-3}$] of the gas-phase opacity species, $\rho$ is the local gas density in [g cm$^{-3}$]. The frequency-dependent absorption coefficient $\kappa^\mathrm{i}_\nu(T)$ is derived from pre-tabulated, opacity-sampled line lists for each of the gas-phase opacity source i (i = 1 . . . N). The integrals in Eqs. 1 and 2 are evaluated at 5608 sampling points in frequency space which are distributed across the entire wavelength interval $0.2\mu$m . . . $20\mu$m. This distribution samples densest the wavelength ranges were the local Planck functions between 1000K . . . 6000K peak. These Planck functions are meant to cover a range of local temperatures where molecules are important opacity sources. For more details see Helling & Jørgensen (1998). Helling & Jørgensen (1998) demonstrated that the temperature-pressure structure of M-stars is not affected by the number of sampling points for which the radiative transfer is evaluated if changed from ∼22 000, to 5608, to ∼500 points. Differences in the temperature-pressure structures become apparent for carbon-rich models and for low-metallicity but only if the sampling number is as low as ∼500. Carbon-rich model atmospheres and low-metallicity model atmospheres show generally a higher standard deviation with decreasing number of sampling points well below 5000 if looked at the changes in the temperature-pressure structure. However, the evaluation of the integrals in Eqs. 1 and 2 will to some extend depends on the integral dicretization, and hence, on the number of frequency points taken into account.

### 2.2 Gas opacity and gas-phase chemistry data

The number density of the gas-phase opacity species, $n_\mathrm{i}$, is computed for a given temperature, T [K], and total hydrogen number density, $\mathrm{n_H}$ [cm$^{-3}$], assuming chemical equilibrium for 14 elements (H, He, C, N, O, Si, Mg, Al, Fe, S, Na, K, Ti, Ca) and 158 molecules with equilibrium constants fitted to the thermodynamical molecular data of the electronic version of the JANAF tables (Chase et al. 1986). The equilibrium constant for TiC are from Gauger et al. (see Helling, Winters & Sedlmayr 2000), for CaH from Tsuji (1973), and FeH from Burrows (2008, priv. com.). First ionisation states of the elements are calculated. The element abundance data are those of Grevesse, Asplund & Sauval (2007), and are summarised in Table 1, otherwise will be stated (see Sect. 3.1.2). The element abundance are adjusted according to the metallicity [M/H]′, the C/O, or the N/O if needed (Sect. 2.3).

We include continuum opacity sources (HI (Karzas & Latter 1961), H- (John 1988), H+H (Doyle 1968), $H_2^-$ (Somerville 1964), $H_2^+$ (Mihalas 1965), HeI (Peach 1970), He- (Carbon et al. 1969), and CI, MgI, AlI, and SiI (Peach 1970). Thomson scattering and Rayleigh scattering for HI and HeI (Dalgarno 1962)). The line opacity sources are taken from the Copenhagen SCAN data base (CO (Goorvitch 1994), TiO (Jørgensen 1994b), SiO (Langhoff & Bauschilder 1993), $H_2O$ (Jørgensen & Jensen 1993), CH (Jørgensen et al. 1996), CN (Jørgensen & Larsson 1990), $C_2$ (Querci, Querci & Tsuji 1974), $C_3$ (Jørgensen et al. 1989), HCN and $C_2H_2$ (Jørgensen 1990 in an updated version), $H_2$-$H_2$ and $H_2$-He collision induced absorption from Borysow (2002 and priv. com.), and were extended (Schnabel 2001) by the HITRAN data base ($CH_4$, $NH_3$, $CO_2$, $SO_2$, $NO_2$, NO, OH, $N_2$; Rothman et al. 2003). Line list from all these data were opacity sampled according to Helling & Jørgensen (1998).

In the most general sense, the opacity data can only be as good as the line-list data are. To access the quality of line lists, studies were undertaken to which extant different line lists can help to fit observed spectra. For example, Jones et al. (2002) used

**Table 1.** Element abundances, $\epsilon_\mathrm{el} = \epsilon_\mathrm{el}^\mathrm{GrAsSa}$ =, from Grevesse, Asplund & Sauval (2007) for calculating the gas-phase chemistry.

| Element | $\epsilon_\mathrm{el}$ | Element | $\epsilon_\mathrm{el}$ |
|---|---|---|---|
| H | 12.00 | Al | 6.37 |
| He | 10.93 | Si | 7.51 |
| C | 8.39 | S | 7.14 |
| N | 7.78 | K | 5.08 |
| O | 8.66 | Ca | 6.31 |
| Na | 6.17 | Ti | 4.90 |
| Mg | 7.53 | Fe | 7.45 |

Phoenix model atmosphere structures and different water line lists to produce synthetic M-dwarf spectra in comparison to observations. Jørgensen (2003) discusses, amongst other molecules, the completeness of $H_2O$-line list data, and its implications for comparisons as in Jones et al. (2002). In addition to the line lists used in this paper, various other line lists are available also for TiO (Plez 1998, Schwenke 1998) and HCN (Harris et al. 2002, 2008; see also Jørgensen 2005). The HITRAN spectroscopic data are regularly updated (Rothman et al. 2005) but the data used cover a maximum temperature interval of ∼ 400 . . . ∼ 3000K only. They were initially compiled for planetary systems. Much work is done to compile more complete line lists, one example being $CH_4$ (Borysow et al. 2003, Nassar & Bernath 2003, Rothman et al. 2005) for which Homeier, Hauschildt & Allard (2003) present a line list data comparison. It therefore needs to be appreciated that the line-list date we are using are incomplete. We tested the effect of missing weak lines and uncertainties thereof (e.g line strength) on the calculation of mean opacities. We artificially increased the line opacity for lines below a certain threshold. Two cases are shown in Fig. 4: (i) all wavelength with $\kappa(\lambda) < 10^{-2}$cm$^2$/g were enhanced by a factor of 3, and (ii) all wavelength with $\kappa(\lambda) < 10^{-5}$cm$^2$/g were enhanced by a factor of 10. These thresholds are small compared to the strongest $H_2O$ or TiO line of $\kappa(\lambda) = 1 - 10$cm$^2$/g at e.g. T≈ 2000K and $\rho \approx 10^{-9}$g/cm$^3$. Figure 4 demonstrates that possibly incomplete line lists have the largest effect on the Rosseland mean opacities since it is dominated by transparent spectral regions due to the harmonic nature of the averaging process (Eq. 1). Therefore, uncertainties in weak-line opacities do have a considerable influence in particular on the Rosseland mean opacities for a tentative line opacity threshold of $\kappa(\lambda) \lesssim 10^{-2}$cm$^2$/g. At temperatures below 1000K uncertainties in the line opacities become noticiable already at a level of $\kappa(\lambda) < 10^{-5}$cm$^2$/g.

### 2.3 Grid values

All mean opacities are calculated for a grid of 71 × 71 temperatures, T, and hydrogen number densities, $n_\mathrm{H}$. The values of $T$ running from 1000K to 10000K, and $n_\mathrm{H}$ running from $1.0\,10^{17}$cm$^{-3}$ to $1.0\,10^{2}$cm$^{-3}$. We calculate mean opacities for varying input element abundances. We vary the C/O ratio, a value which drastically alters the system's chemistry as it passes unity, the N/O ratio which also affects the abundance of the resulting molecular species, and the metallicity [M/H]′. Carbon in particular is important here, as it may well be from low/intermediate mass stars which pass through the AGB phase that the majority of carbon is synthesised (Chiappini, Romano & Matteucci 2003). of particular interest for modelling high-mass stars (S. Campbell, priv. com.).

The abundance of an element is taken to be $\epsilon_\mathrm{el} = \log(N_\mathrm{el}/N_\mathrm{H})+12.0$ (ie. $\epsilon_\mathrm{H} = 12.0$). Then, the ratio of the element in question

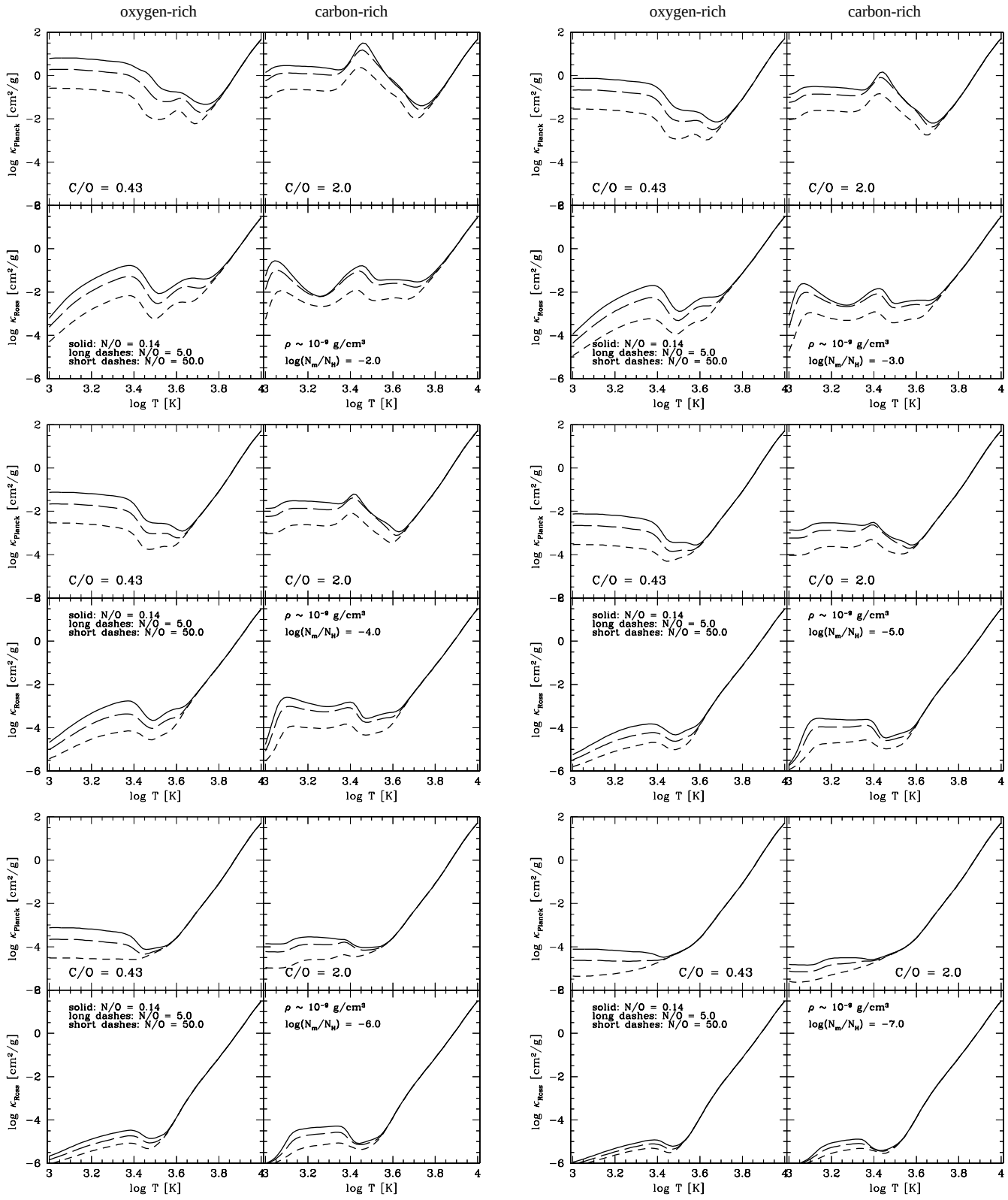


**Figure 1.** Oxygen-rich (C/O=0.43) and carbon-rich (C/O=2.0) gas-phase mean opacities for varying nitrogen abundance (N/O=0.14, 5.0, 50.0). Each set of four plots corresponds to a different metallicity, with values [M/H]′ = -2.0, -3.0, -4.0, -5.0, -6.0 and -7.0. The data is shown for a hydrogen number density $n_{\rm H} = 1.931 \times 10^{15}{\rm cm}^{-3}$ ($\rho \sim 10^{-9}{\rm gcm}^{-3}$).

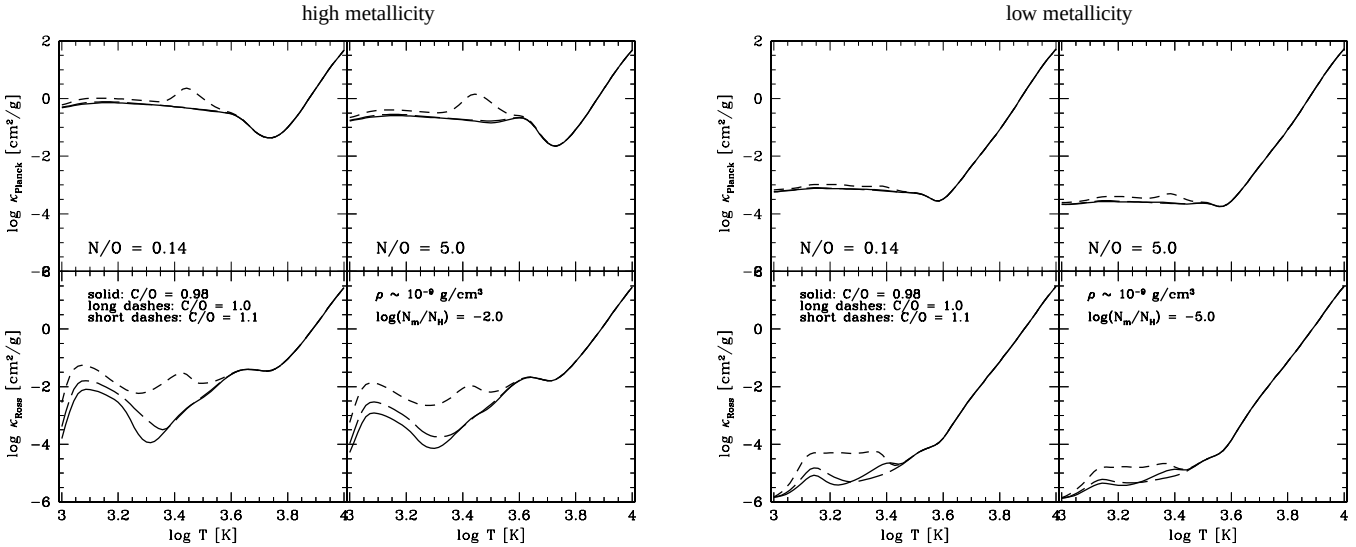


**Figure 2.** Gas-phase mean opacities for the carbon-to-oxygen-rich transition at C/O $\approx$ 1. The left set shows a high metallicity case ([M/H]′ = -2.0), and the right a low metallicity case [M/H]′ = -5.0) both for N/O=0.14, 5.0 for $n_{\rm H} = 1.931 \times 10^{15}$ cm$^{-3}$.

**Table 2.** Grid values of C/O, N/O and [M/H]′ for mean opacity tables.

| | |
|---|---|
| C/O | 0.43, 0.80, 0.90, 0.98, 1.0, 1.1, 2.0, 10.0, 50.0, 100.0 |
| N/O | 0.14, 0.50, 1.0, 2.0, 5.0, 50.0, 100.0 |
| [M/H]′ | −2.0, −3.0, −4.0, −5.0, −6.0, −7.0 |

(here: C, N or all if metallicity is changed) to oxygen can in turn be given as el/O = $10^{\epsilon_{\rm el}-\epsilon_{\rm O}}$. We change the table values (Table 1) for $\epsilon_{\rm C}$ and $\epsilon_{\rm N}$ to give the desired C/O and N/O ratios, for example setting $\epsilon_{\rm C} = \epsilon_{\rm O}$ + log(C/O). This also changes the overall metallicity. We define the metallicity as [M/H]′ = log($N_{\rm M}/N_{\rm H}$), where $N_{\rm M}$ is the total number density of all the atoms heavier than He. Therefore, [M/H]′ = 0.0 is the metallicity such that the total number of metal atoms equals the number of hydrogen atoms. Hence, for a desired metallicity each metal must be modified by $\epsilon_{\rm el}^{\rm new} = \epsilon_{\rm el}^{\rm old} + \log(\beta)$ with $\beta = 10^{[{\rm M/H}]'} \cdot (N_{\rm M}^{\rm old}/N_{\rm H})^{-1}$. The same applies if we vary the C- and the N-abundance (M=C, N) values only. Note that our metallicity is *not* given relative to the solar values but is an absolute value. The relative metallicity values, [M/H], would write [M/H]=[M/H]′−[M/H]$_\odot$ with [M/H]$_\odot$ the solar metallicity (see Sect. 3.1.2).

The grid of values for the metallicity and C/O and N/O ratios are shown in Table 2. The large number of C/O and N/O values should allow models to use the opacity tables for a number of different purposes, like star and planet formation or disk simulations.

We note, that our opacity tables are calculated for a hydrogen-rich environment (with the solar abundances as reference) in contrast to the helium-rich environment of e.g. white dwarfs. Hence, we have not changed the relative abundance of hydrogen to helium, and we also refrain from adopting a non-ideal equation of state. For example, Harris et al. (2004) demonstrate the influence of $HeH^+$ on the opacity of a helium-rich atmosphere. $HeH^+$ is, hence, suggested as an important opacity source for metal-free Population III stars. Also $H_3^+$ was appreciated as candidate for efficient cooling in metal-free gases which is, however, not included in our mean opacity calculation.

## 3 RESULTS

### 3.1 Opacity tables

Figure 1 shows plots of several opacity tables for different combinations of the C/O and N/O ratios, and the metallicity (Table 2). The effects of increasing the N/O ratio and decreasing the metallicity are clearly seen to produce an overall reduction in the mean opacities. The effect due to metallicity can be explained as the fewer metals are present, the fewer complex molecules can form, hence, decreasing absorption coefficient. The effect of changing metallicities on the mean opacity values dominates over the changes in C/O or N/O.

One interesting change is seen in the carbon-rich Rosseland mean. The two strong opacity peaks in the lower temperature region grow smaller as the metallicity is lowered. Eventually, however, they, and the trough between them, form a distinctive plateau by [M/H]′ = −5.0. In the ultra-low metallicity cases of [M/H]′ = −6.0, −7.0, the opacities' features are lessened even more, so that by [M/H]′ = −7.0 both the Planck and Rosseland means are very low and almost constant before the increase due to the continuum opacity sources begins to dominate at about log($T_{\rm g}$) ~ 3.5. This increase at high temperature is seen in all data, but the lower the metallicity the lower the temperature at which it can be seen due to the drop in molecular contribution to the opacity.

Interesting to note is that increasing the N/O ratio also appears to lower both the Planck and Rosseland mean opacities considerably. It should however be taken into consideration that by increasing the nitrogen content, the other metals' abundances will be decreased accordingly in order to agree with the given metallicity. The changes by increasing the relative nitrogen abundance is complex because it extensively affects the chemical composition of the gas phase (Sect. 3.2).

#### *3.1.1 The oxygen-to-carbon-rich transition at C/O≈ 1*

The dichotomy between oxygen-rich (C/O < 1) and carbon-rich (C/O > 1) opacities is very noticeable. This is mainly due to the locking of the majority of either carbon or oxygen, whichever is

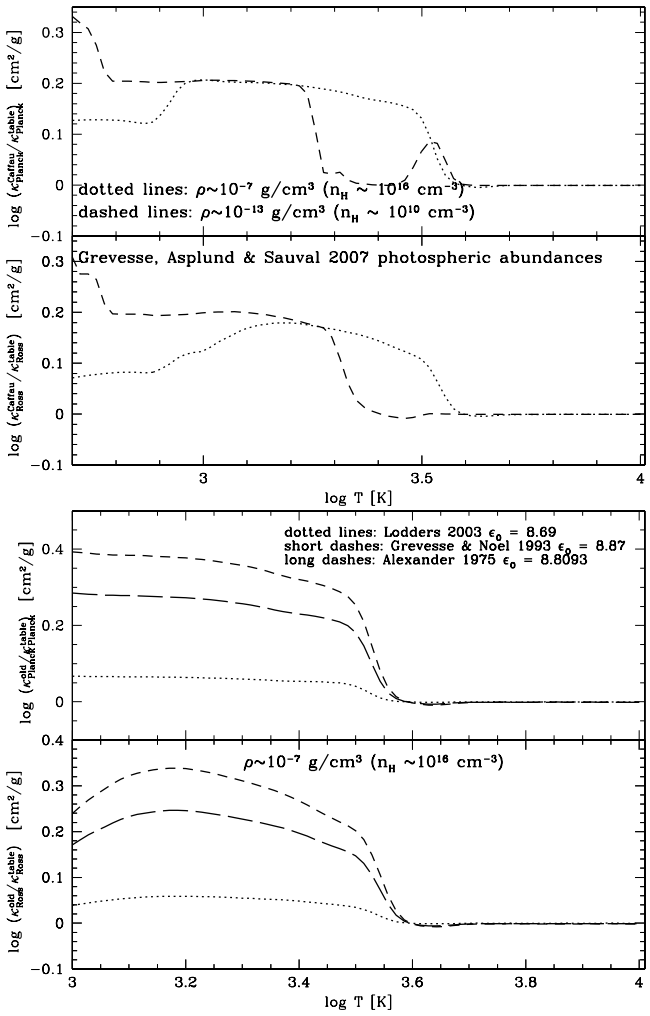


**Figure 3.** Differences in Planck mean and Rosseland mean (top panel) opacities using different oxygen abundance (Grevesse, Asplund & Sauval 2007 $\epsilon_{\rm O}^{\rm GrAsSa} = 8.66$; Caffau et al. 2008 $\epsilon_{\rm O}^{\rm Caffau} = 8.76$). The logarithmic ratio of the opacities is plotted against temperature. In the lower panel, differences in the mean opacities are also shown for the oxygen abundance recommended by Lodders (2003, $\epsilon_{\rm O} = 8.69$), Grevesse & Noel (1993, $\epsilon_{\rm O} = 8.87$, used in Helling, Winters & Sedlmayr 2000), and Alexander (1975, $\epsilon_{\rm O} = 8.8093$). Note that changing the oxygen abundance results in changes of C/O, N/O and [M/H]′. See text for details.

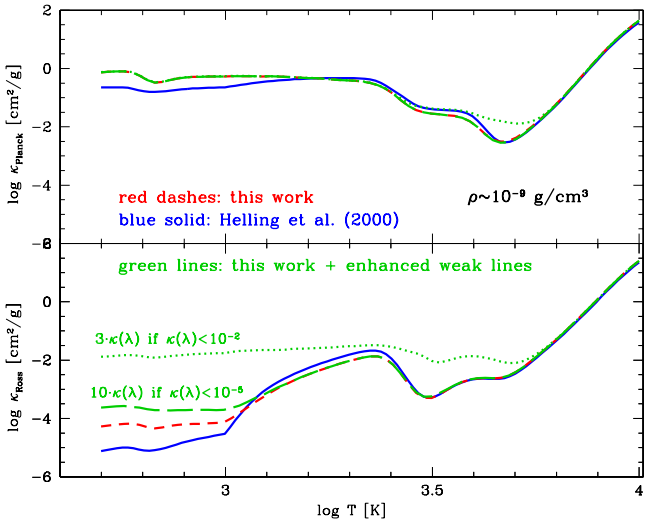


**Figure 4.** Comparing mean opacities of this work (red dashes) to Helling, Winters & Sedlmayr (2000, blue solid). In comparison, the effect of weak-line opacities is shown for two cases (green dots and green long dashes; for details see Sect. 2.2).

the least abundant, in CO. This leaves comparatively little to form other molecules, while the more abundant of the two elements may do so freely. The changes that occur as C/O passes 1.0 can be seen in more detail in Figure 2. Here little difference is seen between the C/O ratios of 0.98 (solid lines) and 1.0 (long dashed lines), particularly in the Planck means. With these ratios, little of either element will be available. Meanwhile, at C/O = 1.1 (short dashed lines) a large difference is seen as it becomes possible for carbon to form opacity-source molecules. Changes in the nitrogen abundances do not affect the mean opacities at C/O≈ 1.

Figure 2 demonstrates that the Planck mean values are only mildly affected by the drastic chemistry changes in the oxygen-to-carbon-rich transition, but the Rosseland mean values do change in particular at low temperatures. This is an indication that line opacity sources with a large number of weak lines (like OH, CH, CN or HCN) are important opacity carrier here. The dramatic effect on the atmosphere structure for the oxygen-to-carbon-rich transition has been discussed for instance in Jørgensen (1994a).

### *3.1.2 The oxygen abundance*

We show how modifying the oxygen abundance affects the resulting gas-phase mean opacities. Two sets of opacity tables were made where only the oxygen abundance differ. We test how our mean opacities change if we use $\epsilon_{\rm O}^{\rm Caffau} = 8.76$ suggested by Caffau et al. (2008) in comparison to $\epsilon_{\rm O}^{\rm GrAsSa} = 8.66$ suggested by Grevesse, Asplund & Sauval (2007). Both values are lower than the previously used oxygen abundance in Helling, Winters & Sedlmayr (2000; see their Table A1). We use the Grevesse, Asplund & Sauval (2007) solar photosphere abundances as specified in Table 1 for all other element abundances. Important to note is that while using the Grevesse, Asplund & Sauval (2007) value of $\epsilon_{\rm O}^{\rm GrAsSa} = 8.66$ the C/O and N/O ratios and the metallicity are: C/O = 0.537, N/O = 0.132, $[{\rm M/H}]_{\odot}^{\rm GrAsSa} = -3.02$. While using the Caffau et al. (2008) values $\epsilon_{\rm O}^{\rm Caffau} = 8.76$, they are: C/O = 0.427, N/O = 0.105, $[{\rm M/H}]_{\odot}^{\rm Caffau} = -2.97$, simply because adding oxygen means adding a metal.

Figure 3 plots for two different gas densities the ratio of the mean values for both calculations with different oxygen abundances. As expected, the mean opacities for $\epsilon_{\rm O}^{\rm Caffau}$ are higher then for $\epsilon_{\rm O}^{\rm GrAsSa}$ since more oxygen is available to form molecules which are opacity sources. Figure 3 (top panel) shows that there is a large disparity when changing between the different oxygen abundances. While the high-temperature Rosseland and Planck mean values are the same since determined by atomic/ionic continuum opacities, the deviations can be as large as 20%–30% in the low-temperature regime where molecular line absorption dominates the total opacity. As research into these abundances values is ongoing, tables using both values were calculated.

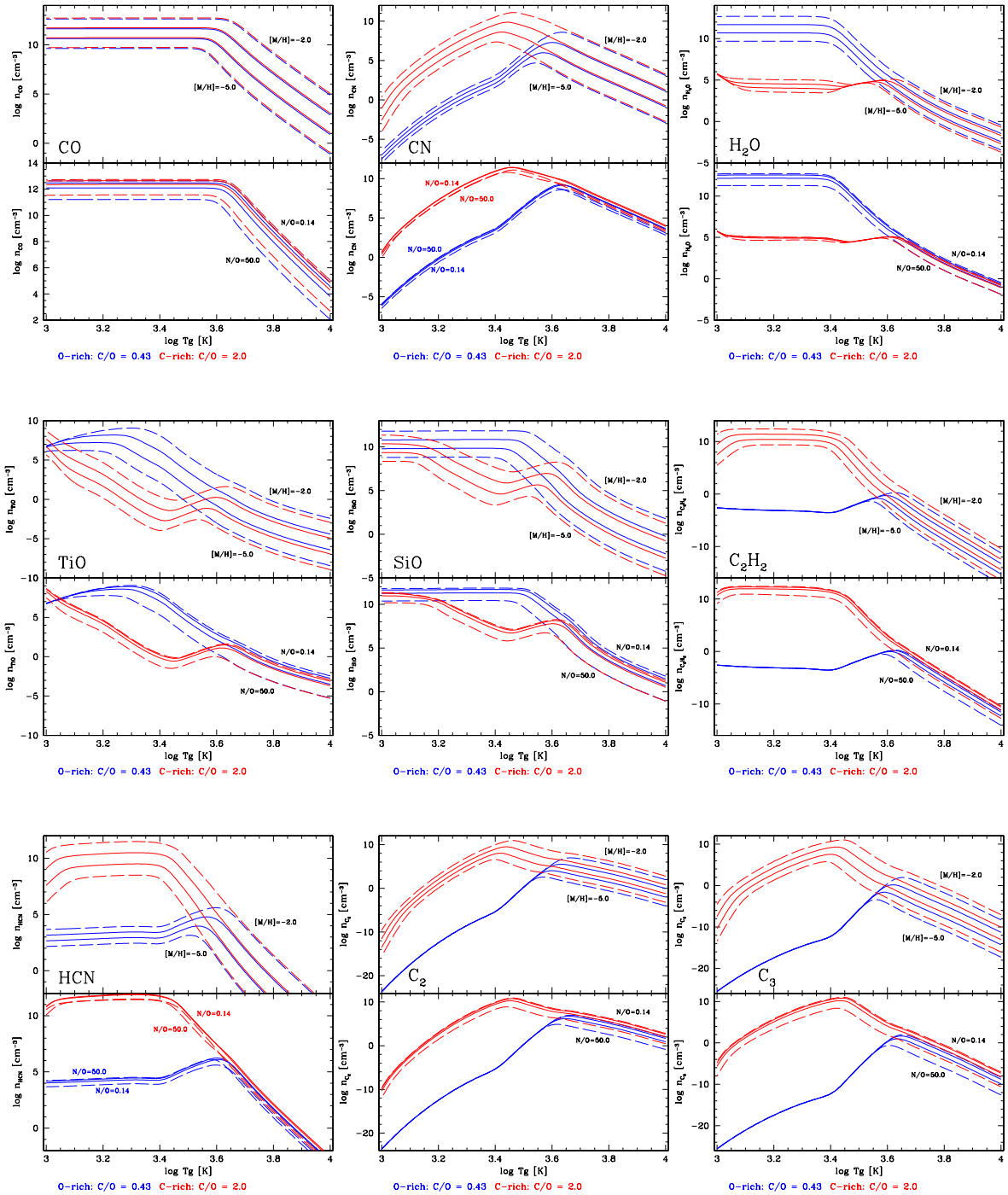


**Figure 5.** Number densities of the line-opacity molecules. The top panels show variation with metallicity, and the bottom variation with N/O ratio ($n_{\rm H}$ = $1.931 \times 10^{15}$ cm$^{-3}$). Dashed lines are labelled with their associated values. Solid lines have [M/H] = 3.0 and 4.0 and N/O = 1.0 and 5.0. Each plot contains values for C/O=2.0 (red) and C/O=0.43 (blue). Note the scales and ranges of each plot are different.

### *3.1.3 Comparing to earlier calculations*

We compare our new mean opacity tables to tables calculated with oxygen abundances suggested by earlier works (Fig. 3, lower panel):

| | |
|---|---|
| $\epsilon_{\rm O}^{\rm Lodders} = 8.69$ | Lodders (2003) |
| $\epsilon_{\rm O}^{\rm GrNo} = 8.87$ | Grevesse & Noel (1993) |
| $\epsilon_{\rm O}^{\rm Alexander} = 8.8093$ | Alexander (1975, King mixture IVa), |

and to tables from Helling, Winters & Sedlmayr (2000) for a collection of Anders & Grevesse (1989) and Grevesse & Noel (1993) abundance data (Fig. 4). The oxygen abundance in these old tables is $\epsilon_{\rm O}^{\rm GrNo} = 8.87$ (Grevesse & Noel 1993). For an update of Lodders (2003) see Lodders, Palme & Gail (2008). The lower panel in Fig. 3 demonstrates that for a given gas density the $\epsilon_{\rm O}^{\rm GrNo}$ mean opacities

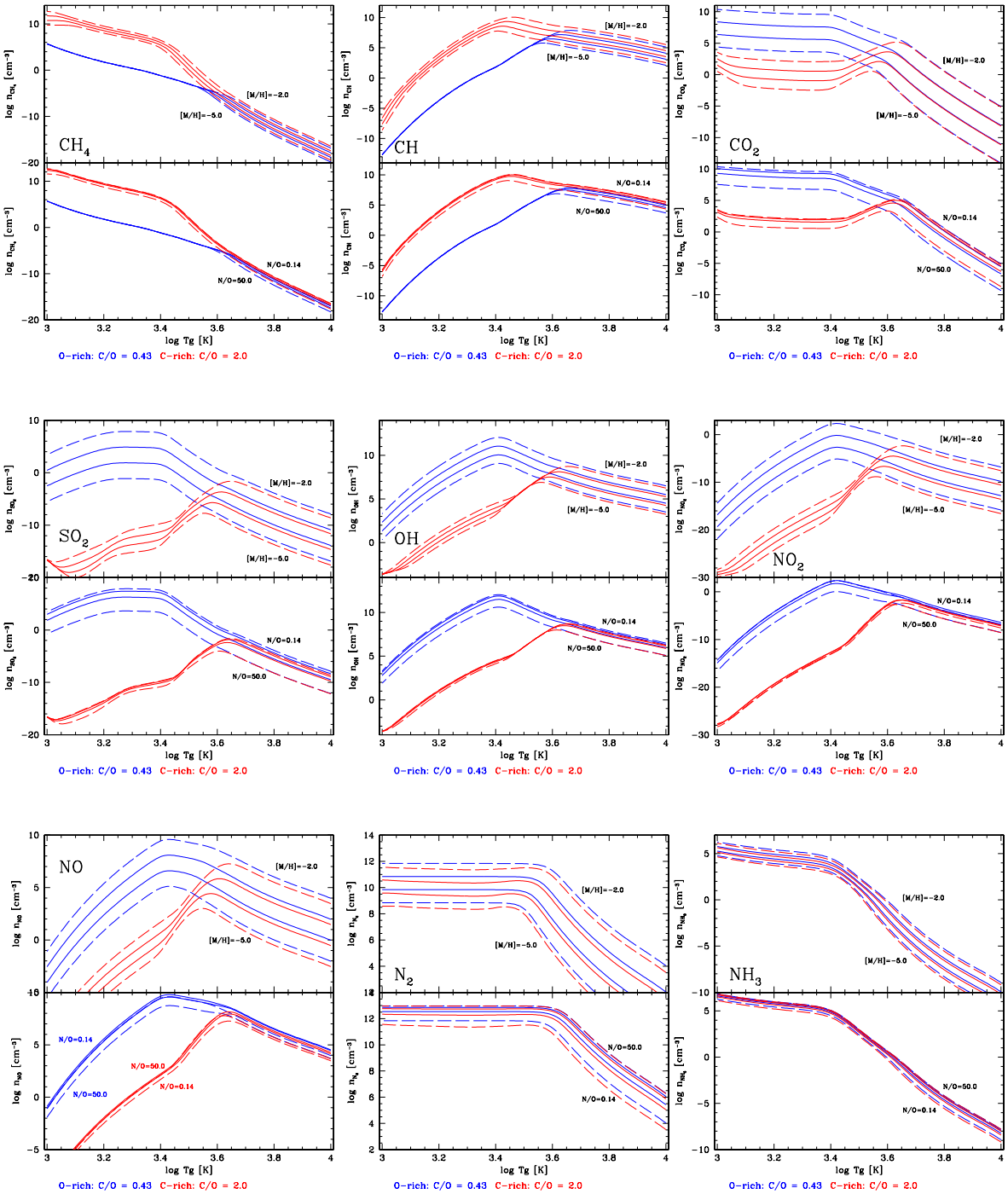


**Figure 6.** Figure 5 is continues here. Several molecules containing nitrogen are shown, which demonstrate a dependence on N/O different from the other molecules.

deviate by up to 40% in the low-temperature ranges from mean opacities calculate using the Grevesse, Asplund & Sauval (2007) atmospheric oxygen abundance value. Our mean opacity results for the Alexander (1975) $\epsilon_{\rm O}$-value fall in-between the results for $\epsilon_{\rm O}^{\rm Lodders}$ and $\epsilon_{\rm O}^{\rm GrNo}$ which is consistent with the comparison shown in Semenov et al. (2003, their Fig. 3 left).

The use of the up-dated element abundances by Grevesse, Asplund & Sauval (2007) and Caffau et al. (2008), and the use of additional opacity sources from the HITRAN data base (Sect. 2.2), causes differences of the present mean opacity values compared to our earlier results (Helling, Winters & Sedlmayr 2000). The additional HITRAN-data mainly affect the mean opacity values below 1000K. Figure 4 (solid blue vs. red dashed) demonstrates that the maximum total difference is 1 – 0.5 orders of magnitude at such low temperatures. Semenov et al. (2003, see their Fig. 2) present a comparison of our Rosseland and Planck mean gas-opacity data

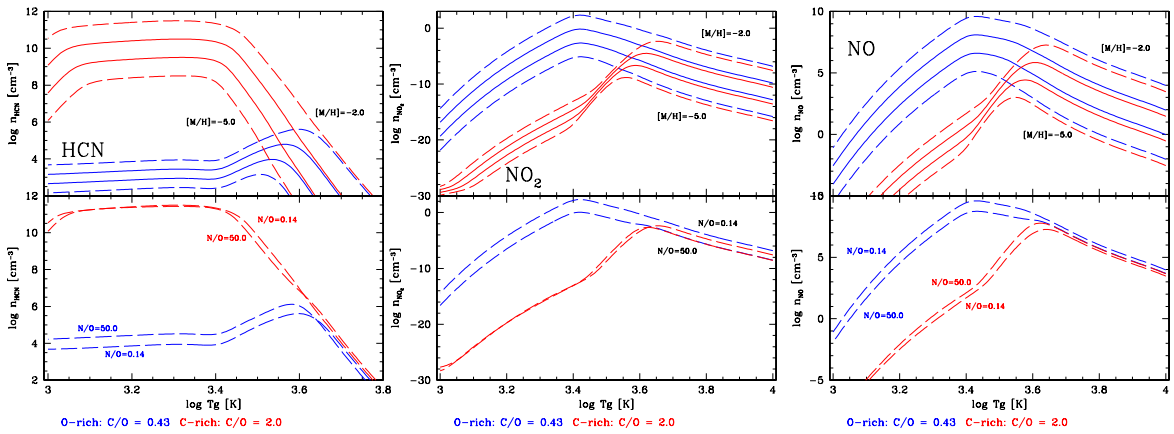


**Figure 7.** Numbers densities for opacity molecules displaying unusual dependence on N/O. Results are only shown for N/O = 0.14 and 5.0, making it easier to see how they vary. HCN and $NO_2$ show that the lines for each N/O may cross one another several times.

to other works including Alexander (1975). The influence of the element abundances on the mean opacities is discussed above with emphasis on the uncertainty in the oxygen abundances. Note, however, that all element abundances taken from Grevesse, Asplund & Sauvale (2008) are lower then in Helling, Winters & Sedlmayr (2000, see their Table A1) including the carbon abundances.

Figure 4 further suggests that possible uncertainties in weak-line opacity data can have a considerably larger influence on the mean opacities than the uncertainties in the element abundances. However, the purpose of our simple weak-line experiment in Fig. 4 was to demonstrate the possible influence on the mean opacity calculation rather then setting a stringent limit on this effects.

### 3.2 Chemistry

In order to evaluate the opacity carriers individual abundance contribution to the mean opacities, a chemical equilibrium routine was run to produce a separate output which gave number densities of the various species across the temperature range. The chemistry routine considers 158 molecules made of 14 elements, but we only present the output for the 18 opacity species included in our mean opacity calculation. Varying the C/O ratio, the N/O ratio, and the metallicity, allowed the opacity table's features to be probed (Figs. 5 - 7).

The first plot of Fig. 5 shows CO. The density of this molecule is effectively constant until $\log(T_g) \sim 3.6$, after which it falls away. This is true in all cases. Only the height of the plateau and the exact point at which it falls off vary with N/O and metallicity. This shows why the opacity changes so strongly between oxygen- and carbon-rich: Of carbon and oxygen, the least abundant has many of its atoms locked within CO, making it harder to form other molecules containing that element due to its high binding energy.

The result of this is seen for many of the molecules shown in Figs. 5 and 6, which show large variations between the oxygen- and carbon-rich cases. Having $C/O > 1$ result in higher densities for the carbon-containing species, and the same is true for the case when $C/O < 1$ which affects mostly the oxygen-binding molecules. This is entirely as expected. An interesting exception is TiO, where it can be seen that at low temperatures ($\log(T_g) \sim 3.1$) the densities for the carbon-rich case rise above those for the oxygen-rich case, because $TiO_2$ becomes more stable than TiO. Lowering the metallicity shifts the point where the densities for each case cross; the same occurs when increasing N/O. SiO shows similar behaviour, but the rising density as temperature decreases flattens just before the high-C density overtakes high-O. Both molecules, TiO and SiO, can therefore contribute to the absorption of a carbon-rich gas at temperatures below 1000K.

Comparing all the plots, similar features become apparent at certain temperatures. In the carbon-rich case, it can be seen that many molecules' densities have a turning-point at $\log(T_g) \sim 3.4$. CN, $C_2$ and $C_3$ all reach a peak here before falling again, TiO and SiO reach a minimum, and $C_2H_2$ and HCN fall off at the end of a plateau. The exact temperature at which these changes occur seems dependent on the metallicity: in all cases it appears as though decreasing the metallicity shifts the point at which these changes in the molecular abundances occur to lower temperatures.

Looking at the opacity tables for $C/O = 2.0$, a peak is noticed in both the Planck and Rosseland means at $\log(T_g) \sim 3.4$. This is caused by the molecules whose number densities also reach a maximum here. The peak occurring at very low temperatures ($\log(T_g) \sim 3.1$) in the Rosseland mean could be a result of the changing densities of several molecules. At the lower temperature boundary, where the opacity peak can be seen to be rising, the TiO and SiO are at their highest points in the carbon-rich domain, but immediately fall. At the same time, $C_2H_2$ and HCN are increasing to the point where they level out into a plateau. Where they reach this point corresponds to the peak in the opacity table. While these two molecules stay at roughly the same density, the two oxides are removed, lowering the opacity. This holds with Lederer & Aringer (2008) who found that $C_2H_2$ and HCN are the main contributors to their carbon-rich Rosseland mean opacities at these low temperatures.

The oxygen-rich molecule densities show a similar 'characteristic' temperature. At $\log(T_g) \sim 3.4$, $H_2O$, which is before this point constant, falls off very quickly, while TiO reaches a peak. SiO also peaks, but at a point perhaps nearer to $\log(T_g) \sim 3.5$. As in the carbon-rich case, the metallicity shifts the position of the features. The initial plateau in the Planck mean and the prominent peak in the Rosseland mean can be easily seen to result from the initial high densities of $H_2O$, SiO and $SO_2$, and other molecules which reach maxima here such as TiO, OH and NO.

In the Planck and Rosseland means for both C/O cases, a small

rise can be noticed at $\log(T_g) \sim 3.6$. This seems to be due to an interesting rise in the density of molecules containing the least abundant of the two elements, eg. if C/O > 1 then molecules containing oxygen reach a peak at about this temperature, and vice verse. It is important to note that this is the temperature beyond which CO's density is seen to fall away, ie. it begins to dissociate. As this happens, atoms of both carbon and oxygen are released, allowing other molecules to form. However the rising temperature inevitably brings about continued dissociation of these molecules as well, leading to the downwards slope seen on all plots. Some of the peaks at $\log(T_g) \sim 3.6$ are of considerable height, allowing contribution the rise noted in the opacities.

### *3.2.1 Changing nitrogen abundance*

It is also important to note what effects changing the N/O ratio has on the molecular densities, and so on the opacities. It can be seen that for molecules not containing nitrogen, increasing N/O leads to a reduction in the gas density. This is because in order to maintain a defined metallicity, when the nitrogen abundance is increased, the other metals' abundances must be decreased. For those molecules which do contain nitrogen, this is different, and furthermore specific to the species in question. For example, the density of NO (Figure 6) increases with N/O in the carbon-rich case, while in the oxygen-rich case the opposite is true. Figure 7 shows the difference more clearly. Meanwhile, $NO_2$ decreases with N/O in the oxygen-rich case, yet when C/O = 2.0 the relationship becomes very unclear with a seeming dependence on temperature as well as N/O. Despite these more complex relationships, most molecules still decrease in number with increasing N/O, leading to the overall decrease in the mean opacities observed in Figure 1.

Comparing the plots of HCN and $NO_2$ in Figures 5 and 6 with their counterparts in Figure 7, it may be seen that in the carbon-rich cases, and at $\log(T_g) \gtrsim 3.5$ when oxygen-rich, the molecules' number densities are lower at N/O = 0.14 and 50.0 than they are when N/O = 1.0 or 5.0. This suggests an optimal N/O ratio which is associated with a maximum in the number density of nitrogen-containing molecules, and dependent on competition between the abundances of carbon, nitrogen and oxygen. Also note that $NO_2$ remains in very low numbers throughout the whole temperature range. While this molecule has little effect on the mean opacities in the temperature interval considered here ($10^3 \ldots 10^4$K), HCN in particular has a strong influence.

Finally, also included in the opacity calculations were lines by collision induced absorption (CIA) by $H_2-H_2$ and $H_2-He$. These are known to contribute significantly to lower temperature and high pressure opacities, however due to the nature of this kind of absorption it cannot be probed as has been done for the molecular lines. Borysow, Jørgensen & Zheng (1997) demonstrated that collision induced absorption is one of the most important opacity source in the atmospheres of the lowest metallicity stars (their Fig. 6).

## 4 SUMMARY

We present a set of gas-phase Planck mean and Rosseland mean opacity tables applicable for simulations of star and planet formation, stellar evolution, disk modelling at various metallicities of a hydrogen-rich gas. The Rosseland mean values are suitable in hot and dense regions of an absorbing gas, where the mean free path of all photons of arbitrary wavelength is smaller than the characteristic scale height of the gas, and hence, the radiative transfer diffusion approximation holds. Here, the large number of weak absorption lines is well represented by the Rosseland mean opacity values. If the gas becomes optically thin, the diffusion approximation becomes invalid, and single, strong absorbing frequencies may become important and determine the radiative flux. In the limiting case of a missing correlation between the frequency distribution of the flux and the frequency distribution of the opacity, e.g. due to line shifts induced by velocity fields, the Planck mean opacity values can serves as a good approximation.

Tables are produced for C/O= $0.43 \ldots 100.0$, for N/O= $0.14 \ldots 100.0$, and $[M/H]' = \log N_M/N_H = -2 \ldots -7.0$ ($[M/H]=[M/H]'-[M/H]_\odot$, $[M/H]_\odot \approx -3$, see Sect.3.1.2). We have shown that the present uncertainty regarding the oxygen abundance values do affect the mean opacity results. We therefor provide tables for the values from Grevesse, Asplund & Sauval (2007) and for the value from Caffau et al.(2008). We demonstrate the dependence of our mean opacity values on C/O, N/O and metallicity. The oxygen-to-carbon-rich transition range around C/O$\approx$ 1 is particular interesting, and our results demonstrate that weak line opacity sources are important here. We caution, however, that uncertainties in the weak-line opacity data can strongly influence the Rosseland mean opacities at a tentative threshold of $\lesssim 10^{-2}$cm$^2$/g for $\kappa^i(\lambda)$ in Eq. 1.

The opacity tables will be available online under http://star-www.st-and.ac.uk/~ch80/datasources.html.

## 5 ACKNOWLEDGMENTS

We thank the referees for their careful reading and valuable suggestion which considerably improved the manuscript. WL thanks the St Andrews Physics Trust for funding his summer placement at the University of St Andrews. ChH thanks Adam Burrows for sharing his chemical equilibrium constants data for the molecular FeH and CO. The computer support at the School of Physics and Astronomy in St Andrews is highly acknowledged.

## REFERENCES

Alexander D.R. 1975, ApJSS 290, 363
Borysow A. 2002, A&A 390, 779
Borysow A., Chamion J.P., Jørgensen U.G., Wegner C. 2003, In: Hubeny I., Mihalas D., Werner K., APS Conf. Series 288, 352
Borysow A., Jørgensen U. G., Zheng C., 1997, A&A, 324, 185
Caffau E., Ludwig H.-G., Steffen M., Ayres T. R., Bonifacio P., et al. 2008, A&A, 488, 1031
Carbon D., Gingerich O., Latham D 1969, in Low Luminocity Stars, ed. Kumar S., 435
Cayrel R., Depagne E., Spite M., Hill V., Spite F., Francois P., Plez P., Beers T. et al. 2004, A&A 416, 1117
Chase Jr., M.W., Davies C.A., Downey Jr., J.R. et al. 1986, J. Phys. Chem.Ref. Dat., 14(1)
Chiappini C., Romano D., Matteucci F., 2003, MNRAS, 339, 63
Cohen J.G., Christlieb N., McWilliam A., Shectman S., Thompson I., Melendez J., Wisotzki L., Reimers D. 2008, ApJ 672, 320
Dalgarno A., 1962, The Scattering of light by Atomic Systems. Volume III of Spectral Reflectivity of the Earth Atmosphere. Geoph.Corp. of America
Dominik C., Gail H.-P., Sedlmayr E., Winters J.M. 1990, A&A 240, 365

Dorfi E., Höfner S. 1998, in Reviews in Modern Astronomy 11: Stars and Galaxies, ed. ed. Schielicke R.E., Astronomische Gesellschaft, Jena, 147
Doyle R., 1968, Ph.D. Thesis, Harvard University, Harvard, USA
Gail H.-P. Sedlmayr E. 1986, A&A 161, 201
Gautschy-Loidl R., Höfner S., Jørgensen U. G., Hron, J. 2004, A&A 422, 289
Goorvitch D., Chackerian Jr. C., 1994, ApJS 91, 483
Grevesse N, Noels A. 1993, in *Origin and evolution of the elements*, Cambridge University Press, 15
Grevesse N., Asplund M., Sauval A.J., 2007, Space Science Reviews, 130, p. 105
Harris G.J., Larner F. C., Tennyson J., Kaminsky B. M., Pavlenko Ya. V., Jones H. R. A. 2008, MNRAS 390, 143
Harris G.J., Lynas-Gray A.E., Miller S., Tennyson J. 2004, ApJ 617, L143
Harris G. J., Polyansky O., Tennyson J. 2002, ApJ, 578, 657
Helling Ch., 1999, PhD thesis, Technischen Universität Berlin
Helling Ch., Jørgensen U.G. 1998, A&A 337, 477
Helling Ch., Winters J.M., Sedlmayr E. 2000, A&A 358, 651
Homeier D., Hauschildt P.H., Allard F. 2003, In: Hubeny I., Mihalas D., Werner K., APS Conf. Series 288, 357
Höfner S., Gautschy-Loidl R., Aringer B., Jørgensen U. G. 2003, A&A 399, 589
John T., 1988, A&A 193, 189
Jones H.R.A., Pavlenko Y., Viti S., Tennyson J 2002, MNRAS 330, 675
Jørgensen U.G. 2005, In: Barnes III B.G. and Bash F.N. (eds.), ASP Conf Ser. Vol. 336, 269
Jørgensen U.G. 2003, In: Hubeney I., Mihalas D. and Werner K. (eds.), ASP Conf Ser. 288, 303
Jørgensen U.G., Larsson M., Iwamae A., Yu B., 1996, A&A 315, 204
Jørgensen U.G., 1994a, In: Jorgensen U.G. (ed.) Molecules in the Stellar Environment. Springer, Berlin, p. 29
Jørgensen U.G., 1994b, A&A 284, 179
Jørgensen U.G., Jensen P., 1993, J. Mol. Spect. 161, 219
Jørgensen U.G., Larsson M., 1990, A&A 238, 424
Jørgensen U.G. 1990, A&A 232, 420
Jørgensen U.G., 1996, in Molecules in stellar environments, ed. U.G Jørgensen, Springer, Heidelberg, 29
Jørgensen U.G., Almlof J., Siegbahn P.E.M. ApJ 1989, 343, 554
Karzas W., Latter R., 1961, ApJS 6, 167
Koch A., Grebel E.K., Gilmore G.F., Wyse R.F.G., Kleyna J.T., Harbeck D.R., Wilkinson M.I., Wyn E.N. 2008, ApJ 135, 1580
Langhoff S., Bauschlicher Jr. C., 1993, Chem. Phys. Letters 211(4,5), 305
Lodders K., Palme H., Gail H.-P. 2008, EPA, submitted (arXiv:0901.1149v1)
Lodders K. 2003, ApJ 591, 1220
Lederer M.T., Aringer B., 2008, in Guandalini R., Palmerini S., Busso M., eds, IXth Torino Workshop on Evolution and Nucleosynthesis in AGB Stars and the IInd Perugia Workshop on Nuclear Astrophysics, AIP Conference Proceedings, 1001, 11
Marques J.P., Monteiro M. J. P. F. G., Fernandes J. M. 2008, ASS (arXiv:0803.2505v1)
Mihalas D., 1965, ApJS 9, 321
Mollá M., Vílchez, J.M., Díaz, A. I., Gavilán, M. 2007 (astro-ph/0701691)
Nassar R., Bernath P. 2003, JQSRT 82, 279
Nowotny W., Aringer B., Höfner S., Gautschy-Loidl R., Windsteig W. 2005, A&A 437, 273
Peach G., 1970, Mem. R. Astron. Soc. 73, 1
Plez, B. 1998, A&A 337, 495
Querci F., Querci M., Tsuji T. 1974, A&A 31, 265
Rothman L.S., Jacquemart D., Barbe A., Benner D.C., Birk M. et al. 2005, JQSRT 96, 139
Rothman L.S., Barbe A., Benner D.C., Brown L.R., Camy-Peyret C. et al. 2003, JQSRT 82, 5
Schnabel K., 2001, Diploma Thesis, Technical University Berlin
Schwenke D.W. 1998, In: Faraday Discussions No. 109, London, 321
Semenov D., Henning Th., Helling Ch., Ilgner M., Sedlmayr E. 2003, A&A 410, 611
Somerville W.B., 1964, ApJ 139, 192
Tsuji T. 2008, A&A 489, 1271
Tsuji T. 1973, A&A 23, 411
VandenBerg D. A., Edvardsson B., Eriksson K., Gustafsson B. 2008, ApJ 675, 746
Wachter A., Winters J.M., Schröder K.-P., Sedlmayr E. 2008, A&A 486, 497
Woitke P. 2006, A&A 460, L9
Wuchterl G. 2005, in in Reviews in Modern Astronomy 17: The Sun and Planetary Systems - Paradigmes for the Universe, ed. Schielicke R.E., WILEY-VCH, Weinheim, 129